Published in final edited form as:
Hum Mol Genet. 2012 June 15; 21(12): 2713–2724. doi:10.1093/hmg/dds097.

Impaired neurotransmission in ether lipid-deficient nerve terminals

Alexander Brodde[1], **Andre Teigler**[1], **Britta Brugger**[1], **Wolf D. Lehmann**[2], **Felix Wieland**[1], **Johannes Berger**[3], and **Wilhelm W. Just**[1,*]

[1]Heidelberg Center of Biochemistry, University of Heidelberg, 69120 Heidelberg, Germany

[2]German Cancer Research Center (DKFZ), Molecular Structure Analysis (W160), 69009 Heidelberg, Germany

[3]Center for Brain Research, Medical University Vienna, 1090 Vienna, Austria

Abstract

Isolated defects of ether lipid (EL) biosynthesis in humans cause rhizomelic chondrodysplasia punctata type 2 and type 3, serious peroxisomal disorders. Using a previously described mouse model [Rodemer, C., Thai, T.P., Brugger, B., Kaercher, T., Werner, H., Nave, K.A., Wieland, F., Gorgas, K., and Just, W.W. (2003) Inactivation of ether lipid biosynthesis causes male infertility, defects in eye development and optic nerve hypoplasia in mice. *Hum. Mol. Genet.*, 12, 1881–1895], we investigated the effect of EL deficiency in isolated murine nerve terminals (synaptosomes) on the pre-synaptic release of the neurotransmitters (NTs) glutamate and acetylcholine. Both Ca^{2+}-dependent exocytosis and Ca^{2+}-independent efflux of the transmitters were affected. EL-deficient synaptosomes respire at a reduced rate and exhibit a lowered adenosin-5′-triphosphate/adenosine diphosphate (ATP/ADP) ratio. Consequently, ATP-driven processes, such as synaptic vesicle cycling and maintenance of Na^+, K^+ and Ca^{2+} homeostasis, might be disturbed. Analyzing reactive oxygen species in EL-deficient neural and non-neural tissues revealed that plasmalogens (PLs), the most abundant EL species in mammalian central nervous system, considerably contribute to the generation of the lipid peroxidation product malondialdehyde. Although EL-deficient tissue contains less lipid peroxidation products, fibroblasts lacking ELs are more susceptible to induced oxidative stress. In summary, these results suggest that due to the reduced energy state of EL-deficient tissue, the Ca^{2+}-independent efflux of NTs increases while the Ca^{2+}-dependent release declines. Furthermore, lack of PLs is mainly compensated for by an increase in the concentration of phosphatidylethanolamine and results in a significantly lowered level of lipid peroxidation products in the brain cortex and cerebellum.

*To whom correspondence should be addressed at: University of Heidelberg, Heidelberg Center of Biochemistry (BZH), Im Neuenheimer Feld 328, 69120 Heidelberg, Germany. Tel: +49 6221544286; Fax: +49 6221544366; wilhelm.just@bzh.uni-heidelberg.de.

Conflict of Interest statement. None declared.

Europe PMC Funders Author Manuscripts

Introduction

The role ether lipids (ELs) play in cellular physiology is still enigmatic. Cells deficient in the peroxisomal enzymes dihydroxyacetonephosphate acyltransferase (DAPAT) or alkyl dihydroxyacetonephosphate synthase lack ELs including plasmalogens (PLs) (1,2). Although viable, these cells exhibit morphological alterations of the endoplasmic reticulum (ER), Golgi apparatus, caveolae and coated pits and show defects in endocytosis and intracellular distribution of cholesterol. To further explore previously unknown EL functions, we generated an EL-deficient mouse model by targeted deletion of DAPAT (3,4). EL-deficient mice show severe phenotypes including development of cataract, various abnormalities of the central nervous system (CNS) (5) and arrest of spermatogenesis (6), changes that are reminiscent of rhizomelic chondrodysplasia punctata (RCDP) types 2 and 3, human peroxisomal disorders distinguished by isolated genetic defects in EL biosynthesis (7,8). Patients with severe RCDP show magnetic resonance imaging abnormalities the severity of which correlates with the clinical appearance and the level of PLs (7–9). Both RCDP patients and mice with targeted deletion of the DAPAT gene share phenotypes, such as growth retardation, bilateral cataract, motor impairment and defects in myelination (4,5), suggesting these mice to be a useful model system of RCDP.

The defects studied in the cerebellum revealed axonal swellings distinguished by disorganization of septate-like junctions and accumulations of inositol-tris-phosphate receptor-containing ER-like cisternae frequently located close to the nodes of Ranvier. Moreover, patterning of climbing and parallel fibers was severely disturbed, indicating imbalance of the activities of GluRδ2-dependent and voltage-dependent Ca^{2+} channel α1A-dependent synapses (5). Thus, impaired synaptic activities may well contribute to the structural alterations caused by EL deficiency.

In presynaptic nerve terminals (synaptosomes, SYNs), neurotransmitters (NTs) are stored in synaptic vesicles (SVs) (10,11). Release of NTs at the presynaptic active zone occurs through exocytosis of SVs described by the SV cycle consisting of vesicle docking, priming and fusion. SVs of the readily releasable pool sense the increase in cytosolic Ca^{2+} induced by the action potential that opens voltage-gated Ca^{2+} channels (12). Ca^{2+}-bound synaptotagmin acting as Ca^{2+} sensor (13) recruits to assembled soluble NSF attachment protein receptor (SNARE) complexes, reverse the action of complexins clamping the assembled SNAREs (14,15) and initiate fusion, while Sec1/Munc18-like proteins engage the trans-SNARE complexes to direct their fusogenic activity. In the cycle, the NT release is followed by clathrin-dependent endocytosis or reuptake through specific intracellular transport systems (16,17).

Although there is consensus that biological membrane fusion depends on SNARE complexes and Sec1/Munc18-like proteins, conditions are known that induce fusion of pure lipidic membranes. Accumulating evidence suggests that the mechanisms directing fusion of biomembranes and membranes of pure lipids involve common sets of intermediate stages. When fusion is initiated membranes no longer are in a planar bilayer (lamellar) shape, but rather adopt highly curved non-bilayer (non-lamellar) formations (18). Nonlamellar lipids, such as phosphatidylethanolamine (PE) and plasmenylethanolamine have the propensity to

assemble into curved monolayers forming inverted H_{II} hexagonal phases that facilitate fusion (18–21). Fusion proceeds by formation of an initial stalk-like intermediate (22) leading to a hemi-fusion stage distinguished by fusion of the contacting monolayers (19,22). NTs such as monoamines, glutamate (Glu) and acetylcholine (ACh) are taken up from the cytosplasm into SVs by vesicular NT transporters. Transport usually involves exchange of vesicular H^+ for cytoplasmic transmitter. Thus, transport depends on an H^+ electrochemical gradient generated by the vesicular H^+ ATPase (23). Acidification is strongly supported by vesicular chloride channels, indicating the important role of ΔpH in vesicular NT transport. However, NT transporters are differently affected by the H^+ gradient. While ACh transport primarily depends on ΔpH, vesicular Glu transport predominantly depends on the vesicular membrane potential and is less influenced by H^+ exchange (24).

The most representative ELs in the human and rodent brain are PLs of the type alkenylacyl PE (plasmenylethanolamine) accounting for ~ 20% of total brain phospholipids, while alkylacyl phosphatidylcholine (PC) (plasmanylcholine) and alkylacyl PE (plasmanylethanolamine) make up ~2% (25,26). Other physiologically relevant mammalian lipids containing ether-linked alkyl chains are platelet-activating factor (alkylacetyl PC), sulfogalactosyl alkylacylglycerol (seminolipid) abundant in the testis and the lipid moiety of most glycosyl phosphatidylinositol (GPI)-anchored proteins (27–30). GPI-anchored proteins specifically enrich in lipid raft microdomains (LRMs) that in neural and other tissues act as platforms for signal transduction (31). LRMs are highly dynamic ~20 nm structures (32) that in addition to GPI-anchored and other LRM-associated proteins are also enriched in cholesterol, glycosphingolipids and, as recently noted, PLs (4,31,33).

Starting with the idea that developmental defects in the CNS of EL-deficient mice may originate from reduced synaptic activity (5) or impaired functioning of LRMs (34,35), we investigated the Glu and ACh release from control and EL-deficient isolated cortical SYNs. Here, we report that EL deficiency affects the energy state and lipid composition of cortical SYNs resulting in the significant reduction in the NT release. The results may be interpreted as effects of EL deficiency on the imbalance of intracellular ion homeostasis with serious consequences in mitochondrial energy coupling and ER stress response.

Results

Numerous studies have demonstrated the usefulness of synaptosomal preparations to investigate the presynaptic NT release (36). As isolated nerve terminals no longer are subject to depolarization by the action potential, depolarizing conditions applied *in vitro* are, for example, high external K^+ concentrations (30–60 mM) replacing Na^+, inhibition of K^+ channels by 4-aminopyridine or activation of Na^+ channels by veratridine. In this study, we used elevated K^+ that generates a single-clamped depolarization of the plasma membrane opening voltage-dependent Ca^{2+} channels. As a consequence, cytosolic Ca^{2+} levels increase triggering a biphasic, Ca^{2+}-dependent release of NTs (37). Both release of endogenous transmitters (Glu, ACh) and transmitters released following uptake of [^{3}H]-Glu or [^{3}H]-Ch into isolated SYNs were investigated.

Release of Glu

Glu is released from SYNs by two distinct mechanisms, Ca^{2+}--dependent exocytosis and Ca^{2+}-independent efflux from the cytoplasm. To distinguish between both mechanisms, two separate determinations were carried out, one in the presence of Ca^{2+} measuring both Ca^{2+}-dependent and -independent release, and one in the presence of ethylene glycol tetraacetic acid (EGTA) measuring the Ca^{2+}-independent efflux only.

About 80% of synapses in rodent CNS are glutamatergic. Thus, Glu concentrations in CNS are high and can accurately be determined by a fluorimetric assay linked to the enzymatic production of NADPH. No significant differences in the total brain Glu content were observed (Fig. 1A). Whereas the release of Glu from control and EL-deficient SYNs was about the same in the absence of Ca^{2+} (Fig. 1D), in its presence Glu release from EL-deficient SYNs was significantly reduced by 14% (Fig. 1C), indicating that the 58% reduction seen in EL-deficient SYNs (Fig. 1B) was largely due to reduced Ca^{2+}-dependent exocytosis rather than Ca^{2+}-independent efflux.

A similar difference in Ca^{2+}-dependent release between wild-type and EL-deficient SYNs was noted when the Glu release was analyzed following [^{3}H]-Glu uptake into isolated nerve terminals (Fig. 2B). Total uptake into wild-type and EL-deficient SYNs was not significantly different (Fig. 2A). However, EL-deficient SYNs compared with controls released significantly higher quantities of Glu in the absence (Fig. 2D) but not in the presence of Ca^{2+} (Fig. 2C), resulting in a 45% decrease in Ca^{2+}-dependent exocytosis (Fig. 2B).

To investigate in more detail the availability of Ca^{2+} to the exocytotic machinery, release experiments were conducted using the $Ca^{2+}/2H^+$ ionophore ionomycin. When ionomycin at a concentration of 5 μM was added to the SYN suspension 1 min prior to Ca^{2+} (Fig. 3B) or EGTA (Fig. 3C) and 4 min prior to K^+ elevation, Ca^{2+}-dependent Glu exocytosis in EL-deficient SYNs was reduced by 45% when compared with the wild-type (Fig. 3A). Furthermore, the quantity of Glu released from both wild-type and EL-deficient SYNs increased by a factor of three compared with the release without ionophore, suggesting additional Ca^{2+} availability generated by the ionophore (Figs 1B and 3A). Interestingly, while ionomycin in the absence of Ca^{2+} was without effect on wild-type SYNs (Fig. 1D and 3C), in EL-deficient ones it caused a >50% increase in Glu release (Fig. 3C). Thus, the difference between wild-type and EL-deficient SYNs in Ca^{2+}-dependent exocytosis mainly has to be ascribed to this increase in Ca^{2+}-independent efflux.

Release of ACh

Release of both endogenous ACh and [^{3}H]-ACh synthesized following [^{3}H]-Ch uptake was determined in wild-type and EL-deficient SYNs by a similar protocol as used for the Glu studies. Endogenous ACh was determined by the luminometric choline oxidase assay (inset to Fig. 4) following the ACh esterase cleavage (38). Ca^{2+}-dependent ACh release induced by high external K^+ and determined as the difference in the presence and absence of Ca^{2+} was significantly reduced by 50% in EL-deficient SYNs (Fig. 4). No significant difference was seen between wild-type and EL-deficient SYNs in both uptake of [^{3}H]-Ch and release of [^{3}H]-ACh from prelabeled SYNs in the presence of Ca^{2+} (Fig. 5A and C). However, Ca^{2+}-

independent efflux of [^{3}H]-ACh was remarkably increased in EL-deficient SYNs (Fig. 5D) resulting in a significant 32% reduction in Ca^{2+}-dependent [^{3}H]-ACh exocytosis (Fig. 5B).

In summary, exocytosis of both endogenous ACh and Glu was reduced in EL-deficient SYNs by ~60%, respectively (Fig. 6A). Following uptake of [^{3}H]-labeled Glu or Ch, the Ca^{2+}-dependent release of [^{3}H]-Glu and [^{3}H]-ACh was impaired in EL-deficient SYNs by 47 and 31%, respectively (Fig. 6B).

Synaptosomal energy requirement

As exocytosis of NTs from SYNs is an energy-consuming process (39), we analyzed the respiratory capacity of free cortical mitochondria and SYNs using a Clark-type electrode. The rate of respiration of free wild-type and EL-deficient mitochondria neither in the absence nor presence of additional substrates, such as succinate or succinate plus adenosine diphosphate (ADP) was significantly different (Fig. 7A). However, synaptosomal respiration differed from that of free mitochondria in two respects. First, in the medium containing 10 mM glucose EL-deficient SYNs respired at a rate 28% decreased compared with wild-type SYNs (Fig. 7B). Secondly, upon depolarization in the presence of Ca^{2+} the rate of respiration of wild-type SYNs increased significantly, whereas EL-deficient SYNs completely failed to adapt respiration to the consequences of depolarization (Fig. 7B). According to the reduced respiratory capacity of EL-deficient SYNs, the adenosin-5′-triphosphate (ATP) content was also significantly diminished by 27%, while ADP concentrations in wild-type and EL-deficient SYNs were largely the same. As a consequence, the ATP/ADP ratio in EL-deficient SYNs was decreased by 23% (Table 1). Thus, the lack of synaptosomal ELs caused an impaired energy balance that might well contribute to the disturbed NT exocytosis.

Analysis of synaptosomal lipids

Presynaptic signaling depends on membrane-localized processes, such as vesicle exocytosis and functioning of various ion channels and pumps. Therefore, we investigated by lipidomic analysis the impact of EL deficiency on synaptosomal membrane lipid composition (Table 2 and Supplementary Material, Table S1). In wild-type SYNs, PLs contributed to total lipids by 14%. Their lack in mutants caused an increase mainly in the concentration of PE by ~50% raising the percentage of PE from 17% in wild-type to 28% in EL-deficient SYNs. In spite of the general increase in PEs, the major PE species in wild-type SYNs PE 40:6 decreased, whereas PE 38:4 increased more than 2-fold in concentration in EL-deficient SYNs. Although there were remarkable changes in the relative concentrations of PEs, the concentration of polyunsaturated fatty acids (PUFAs) in total synaptosomal membranes of EL-deficient SYNs were fairly the same (292.91 nmol/mg of the protein) as that in the wild-type (321.36 nmol/mg of the protein). A similar tendency as seen in isolated SYNs was to be observed in LRM preparations where PLs contributed 23% to total lipids. EL deficiency led to an increase in PE from 8% in the wild-type to 22% in EL-deficient LRMs. All PE species were increased in EL-deficient LRMs by factors between 1.6 (PE 38:6) and 4.1 (PE 36:2) except PE 40:6 that remained in concentration as in wild-type LRMs. Again PE 38:4 was the dominant species in EL-deficient LRMs.

EL deficiency also caused subtle changes in the relative proportion of various PC, SM and PS species (Supplementary Material, Table S1). PC concentrations decreased by ~10% both in intact SYNs and their LRMs. Interestingly, PC 38:6 and PC 40:6 were lowered in EL-deficient SYNs and their LRMs to about half the amount present in wild-type, suggesting fine-tuning of the synaptosomal membrane fluidity. SM slightly increased and became enriched in LRMs by a factor of about 3. For PS, we recognized in LRM preparations of both wild-type and EL-deficient SYNs a remarkable increase in the concentration of the less-unsaturated species PS 36:1 at the expense of PS 40:6, suggesting PS to be involved in regulating of LRM fluidity.

Oxidative stress in EL-deficient tissues

PLs are known to be more susceptible to oxidative attack than normal phospholipids. This observation led to the proposal of PLs to protect cells from oxidative stress (1,26,40–42). As most of the studies dealing with this subject were carried out *in vitro*, we investigated the anti-oxidative status of selected PL-deficient tissues in order to correlate potential oxidative tissue damage with the observed impairment of presynaptic transmitter release. To this end, Total reactive antioxidant potential (TRAP), total GSH and GSSG as well as thiobarbiturate-reactive substances (TBARS) were determined.

TRAP measurements provide important information on the capacity of tissues to withstand oxidative stress imbalance. The method usually implies thermolytically generated 2,2′-azobis(2-methylpropionamidine) 2HCl (ABAB) radicals that in the presence of luminol induce luminescence (43). TRAP is usually quantified by estimating the concentration of Trolox, a synthetic antioxidant, producing the same quenching of luminescence as the tissue under investigation. As shown in Figure 8A, the equivalent Trolox concentrations in tissues with and without PLs were the same. Thus, PLs do not significantly add to TRAP of the brain, lung and liver, tissues that have high, intermediate and very low PL concentrations, respectively (25).

Furthermore, we investigated ABAP-induced oxidative attack on the viability of wild-type and EL-deficient mouse fibroblasts. The results demonstrate the concentration-dependent decrease in viability that was significantly more pronounced in cells lacking PLs (Fig. 8B).

Many tissues including the brain contain GSH concentrations that are in the millimolar range (44). The GSH–GSSG system is one of the most important cellular means defending oxidative stress. PL deficiency did not cause a significant change in the level of GSH and GSSG except the slight increase in GSSG in liver where PL concentrations are very low (Supplementary Material, Fig. S1) (25).

TBARS are a widely used marker indicating the extent of cellular lipid peroxidation. The assay largely determines the concentration of malondialdehyde (MDA), a major oxidation product derived from PUFAs (45). Surprisingly, in the CNS of both the cortex and cerebellum, PL deficiency caused a significant reduction in TBARS by ~40%. No such changes were found in the liver and lung (Fig. 9A). As these results were in contradiction to previous reports (41), we further studied iron/ascorbate-induced MDA production in cortical brain homogenates and lipid extracts. In brain homogenates lacking PLs, MDA production

was delayed during the 1 h oxidation period compared with controls, although the observed differences were statistically not significant (Fig. 9B). In line with these experiments, we noted in lipid extracts from PL-deficient cortical tissue significantly less MDA when compared with normal tissue extracts (Fig. 9C). These data suggest that PLs, although not detectably contributing to TRAP, at least in the brain considerably account for the formation of lipid peroxidation products.

mRNA microarray analysis

The remarkable alterations of SYN functions elicited by the deficiency of ELs raised the question as to changes in the expression level of functionally related genes. We therefore initiated microarray analysis comparing mRNA expression profiles of the control and PL-deficient cerebellum. Surprisingly, none of the genes closely related to the phenotypes seen in the PL-deficient brain (5) appeared to be altered. Instead, we found the down-regulated expression of a limited number of mRNAs, such as heat-shock protein 90b1 (Hsp90b1/Grp94/gp96), Hspa5 (BiP/Grp78), protein disulfide isomerase-associated 4 and 6 (PDI4, PDI6), X-box-binding protein 1 (XBP1) as well as arginine-rich mutated in early stage tumors (ARMET) and cysteine-rich with EGF-like domain 2 (CRELD2) (46,47), known to be related to the unfolded protein response (UPR) (48,49) (Supplementary Material, Table S2). These data indicate that PL deficiency by mechanisms that still have to be defined might be implicated in the regulation of the UPR possibly by affecting the IRE1α/XBP1 pathway.

Discussion

Previous studies on the EL-deficient mouse model, particularly those on Purkinje cell innervation, suggested PLs to be required for correct functioning of presynaptic activity. The present analyses of NT release indeed demonstrated that the lack of PLs compromised presynaptic activity by both decreasing Ca^{2+}-dependent and increasing Ca^{2+}-independent release. How are these findings interpreted in terms of PL function? NT release is a strictly ATP-dependent process requiring functional synaptic mitochondria (36). As shown here, EL deficiency caused the reduction in synaptic respiratory activity and consequently the decrease in the ATP/ADP ratio by >20% (Fig. 7, Table 1). This decrease seems to be sufficiently high to account for the observed effects on Glu and ACh exocytosis as documented in a previous study on guinea pig SYNs (50). Inhibition of aerobic respiration by rotenone resulting in the time-dependent decrease in ATP by 25% reduced the Ca^{2+}-dependent Glu exocytosis by ~30% and substantially enhanced the Ca^{2+}-independent Glu release. Quite similar observations were made in EL-deficient SYNs in which respiration and ATP levels were lowered by ~30% resulting in a >40% decrease in Ca^{2+}-dependent exocytosis (Table 1, Fig. 6). The Ca^{2+}-independent increase was particularly striking either for the efflux of Glu by the Ca^{2+} ionophore ionomycin present during depolarization or SYNs were first loaded with [^{3}H]-Glu or [^{3}H]-Ch both raising the free cytoplasmic concentrations of the transmitters (51). A reasonable explanation might be that the lowered energy level impairs the activity of the Na^+/K^+ ATPase that in turn reduces the Na^+ gradient across the plasma membrane. Consequently, the Na^+-dependent Glu transporter, normally implicated in the removal from the synapse of released Glu, reverses, liberating cytoplasmic

Glu in a Ca^{2+}-independent manner (52). The electrogenic nature of the Glu transporter in addition might attenuate the driving force for uptake during membrane depolarization further supporting transport reversal (53). The enhanced Ca^{2+}-independent release of Glu from the pre-synaptic terminal (Figs 2 and 3) and the inability of EL-deficient synaptic mitochondria to respond to the altered ion concentration gradients during depolarization strongly indicate dys-functioning of these mitochondria. As a consequence, their reduced level of ATP will delay recovery of the Na^+/K^+ gradient and result in sustained higher levels of cytoplasmic Ca^{2+}. In a negative feedback, enhanced cytoplasmic Ca^{2+} in turn might have serious consequences to mitochondrial activities, such as regulation of ion homeostasis and energy coupling (54). Moreover, recent lipidomic analysis indicated that brain and heart mitochondria contain significant quantities of PLs (55,56) and thus deficiency of PLs in mitochondria might definitely contribute to the synaptic impairment of EL-deficient SYNs. In addition to the mitochondrial compartment, the ER that is heavily implicated in phospholipid biosynthesis and Ca^{2+} homeostasis might also be affected by the lack of PLs. Surprisingly, cerebellar microarray analyses revealed the down-regulation of components of the UPR in the ER (49), suggesting PL deficiency to bias ER functions. Gene transcripts coding for XBP1, BiP/GRP78, Hsp90b1, PDI4, PDI6, CRELD2 and ARMET/MANF were significantly down-regulated without impairing other components of the UPR, such as IRElα, PERK, ATF4 and ATF6. As the level of BiP determines the activities of PERK, IRE1α and ATF6 (57), ER stress response pathways might be generally affected. Hence, in case of acute stress, cells might be ill-prepared to respond and more susceptible to ER stress-induced death. The reduced level of XBP1 might play a central role in down-regulation of components of the UPR. XBP1 is activated by IRElα to function as a pivotal transcription factor regulating both its own expression and that of BiP (58). In addition, XBP1 has also been shown to trigger lipid biosynthesis and biogenesis of the secretory apparatus (59). Thus, the reduced activity of XBP1 might well account for morphological and possibly functional impairments previously described in ER and Golgi of EL-deficient human skin fibroblasts (2).

The mass spectral lipid analyses of SYNs demonstrated subtle changes in membrane phospholipid composition due to EL deficiency. Particularly, the concentrations of individual species of PE were affected. Most of them increased, notably PE 38:4, while PE 40:6 decreased. These changes in the phospholipid composition obviously compensated for the lack of PLs especially PL 38:5, PL 38:7 and PL 40:7 (Table 2). The subtle changes in phospholipid composition might influence membrane fluidity (1), direct PL–protein interactions (20,60) or the function of 1-O-alkyl moiety-containing GPI-anchored proteins (29). However, to what extent these changes contribute to the overall effects of EL deficiency remains subject to further investigations.

A major role of PLs frequently discussed in the literature is their ability to protect cells against reactive oxygen species (ROS) and to function as endogenous antioxidants (26,61). While *in vitro* experiments accumulated substantial evidence for this function, the role of PLs *in vivo* in antioxidative defense still has to be defined. Oxidants found to elicit PL degradation include peroxyl radicals (62), UV light (26) and various transition metals (40,41,62,63). The labile vinyl ether bond at the sn-1 position of PLs appears to be target of direct oxidant reaction. Concomitantly, the oxidation of PUFAs present in the reaction

mixture directly bound to the sn-2 position of either PLs or other phospholipids (Table 2, Supplementary Material, Table S1) seems to be considerably delayed (40), suggesting PLs to have antioxidative properties. In line with this, the present results on PL-deficient tissue demonstrate significantly less MDA production compared with wild-type tissue supporting the view that PLs are a major source of MDA. Although PL-deficient tissues contain less MDA and possibly other toxic lipid peroxidation products (Fig. 9), such as various aldehydes and hydroxyaldehydes (63), lack of PLs significantly renders cells more susceptible to induced oxidative stress (Fig. 8B) (26,61). These mutually contradictory results might suggest that the continuous generation of ROS keeps cellular oxidative and antioxidative activities in balance. Reduced ROS production down-regulates the protective capacity rendering cells prone to sudden oxidative attack (Fig. 8B).

Materials and Methods

Biological preparations

DHAPAT-null mice were generated as previously described (3,4). The animals were maintained in the breeding facility of the IBF of the University of Heidelberg and kept on a normal diet that did not contain detectable amounts of ELs. Mouse brain SYNs were prepared with slight modifications as described (64). The brain was removed and a 10% cerebral homogenate prepared using a 5 ml Potter homogenizer (0.1 mm clearance) and 10 up and down strokes at 700 rpm in 0.32 M sucrose adjusted to pH 7.4 (1 M HCl) containing ethylenediaminetetrqacetic acid (EDTA)-free protease inhibitors (Roche, Mannheim). Nuclei were removed at 1000*g* for 10 min and the supernatant centrifuged for 25 min at 15 000*g*. The pellet was re-suspended in 2 ml of 0.32 mM sucrose containing 0.25 mM dithiothreitol (DTT) and EDTA-free protease inhibitors adjusted to pH 7.4 and applied to a four-step Percoll gradient consisting of 0.5 ml of 50% (w/v) sucrose and 2.5 ml of 23%, 4.5 ml of 10% and 1.5 ml of 3% (w/v) Percoll dispersed in the same medium and centrifuged for 13 min at 32 500*g*. SYNs were located at the 10%/23% interphase and free mitochondria between 23% Percoll/50% sucrose.

LRMs were prepared as described in reference (65,66). SYNs (2 mg) were washed in the LRM buffer (10 mM Tris, 140 mM NaCl, 1 mM EDTA, 1 mM DTT, pH 7.4), transferred to a SW41 tube and gently mixed with the same amount of LRM buffer containing 2% TX-100. The sample was incubated on ice for 30 min and vortexed every 5 min for 5 s. Using 60% (v/v) Optiprep, the suspension war adjusted to 40% final concentration and overlayed with 5 ml 35% (v/v) Optiprep and 2 ml LRM buffer. Centrifugation was for 3 h at 150 000*g*. LRMs were recovered at the buffer/35% Optiprep interphase.

Transmitter release

Organelles were first reenergized for 20 min at 37°C/900 rpm (67) and subsequently incubated for 3 min at 37°C in the presence of either 1.3 mM Ca^{2+} or 1 mM EGTA before depolarization in the presence of 60 mM KCl for 3 min at 37°C. Samples were centrifuged at 20 000*g* for 5 min and the supernatant stored on ice until assayed. Ionomycin was used at a concentration of 5 μM added 1 min prior to the addition of Ca^{2+}. Glu was measured fluorometrically at wavelengths of 340 and 460 nm by monitoring the production of

NADPH in an enzyme-coupled assay (Glu dehydrogenase type III, Sigma) using 400 µg of SYNs (68). At the end of each assay, 4 nmol Glu were added as an internal standard for quantification. Total Glu content of SYNs was measured by adding Triton X-100 [Roche, Mannheim, final conc. 0.5% (v/v)] to the reenergized samples and incubation for 2 min at 37° C/900 rpm.

To 400 µg reenergized SYNs, 5 µM hemicholinium-3 (Sigma, Munich) was added and ACh release initiated in the presence and absence of Ca^{2+} as described for Glu. ACh was measured enzymatically (choline oxidase *Alcaligenes sp*. and ACh esterase, *E. electricus*, horseradish peroxidase type III, Sigma, Munich) using the luminometric assay as described (38,69). Luminescence was read for 10 s (Berthold Lumat LB 9501). All samples were measured in triplicate.

Release of [^{3}H]-labeled NT

To 300 µg SYNs, 0.5 µCi [^{3}H]-Glu or 2 µCi [^{3}H]-choline ([^{3}H]-Ch) were added and the assays incubated for 15 min ([^{3}H]-Glu) or 30 min ([^{3}H]-Ch) at 37°C/900 rpm. Samples were chilled on ice and centrifuged for 5 min at 11 000*g*. Pellets were washed twice to remove unincorporated radioactivity and the resuspended organelles reenergized for 7.5 min at 37°C/900 rpm. Release was performed as described above for Glu and ACh. Radioactivity was determined by liquid scintillation counting.

Analytical procedures

The protein was determined by a modified Lowry method adding 0.2% SDS to the TCA-precipitated protein (70).

Synaptosomal ATP/ADP content was determined by using the ATP bioluminescence assay kit CLS II (Roche, Mannheim). In brief, 200 µg of SYNs were gently resuspended for re-energetization in 1 ml of HBM and incubated at 37°C at 900 rpm for 2 min (67). Thereafter, the sample was added to 4 ml of lysis buffer (95°C) and incubated for an additional 2 min at 95°C. After chilling on ice, the content was centrifuged for 5 min at 20 000*g* and the supernatant stored on ice. ADP determination was carried out by adding to 1 ml of supernatant 10 U of pyruvate kinase, 2 mM phosphoenol pyruvate and 10 mM MgSO4 and incubating the assay for 15 min at 37°C and 900 rpm. The reaction was terminated by heating to 95°C for 2 min and centrifugation for 5 min at 20 000*g*. To 25 µl of supernatant 175 µl of reaction buffer and 50 µl of luciferase reagent were added and the resulting luminescence read for 10 s (Berthold Lumat LB 9501). All samples were measured in triplicate.

Cholesterol was determined fluorometrically by using the Amplex Red Kit (Invitrogen, Darmstadt) according to the instructions of the manufacturer. In brief, samples containing 1–3 µg of the synaptosomal protein were added to the reaction solutions and incubated for 30 min at 37°C in 96-well plates. Fluorescence intensity was analyzed in a plate reader (Molecular Devices, SpectraMax Gemini XS) at wavelengths of 560 and 590 nm. Measurements were performed in triplicate.

Mass spectrometry analyses were done with a triple quadrupole instrument (QUATTRO II, Micromass) equipped with a nano-ESI source. The source temperature was set to 30°C and according to the ion mode a capillary voltage of ~600–900 V was applied. Lipid extraction was performed as described (71) adding lipid standards dissolved in chloroform/methanol (1:2) before extraction. Dried lipids were re-dissolved in methanol containing 10 mM ammonium acetate. Quantification of PC and SM was carried out as described (72) and PE and PS were determined by neutral loss scanning using a collision energy of 20 eV and selecting for a neutral loss of 141 or 185 Da (positive ion mode), respectively. PL-PE (plasmenyl ethanolamine) was assayed by precursor ion scanning for fragment ions 364, 390 and 392 Da (positive ion mode, using a collision energy of 18–20 eV) (72,73). Lyso-PL-PE was purchased from Matreya (Pleasant Gap, PA, USA). Quantifications were based on the phosphate content (74).

Oxygen consumption of synaptosomal and free brain mitochondria was determined by using a Clark electrode (OROBOROS® Instruments, Cylobios, Oxygraph, Innsbruck, Austria). Measurements were performed in duplicate. Briefly, 750 µg of SYNs or 125 µg of mitochondria were pelleted at 11 000*g* for 5 min and 4°C. SYNs were washed once with the hydroxyethyl piperazylethanesulfonic acid (HEPES)-buffered salt medium (118.5 mM NaCl, 4.7 mM KCl, 0.1 mM Na_2HPO_4, 1.18 mM $MgCl_2$, 20 mM HEPES, 10 mM glucose, pH 7.55) and mitochondria with Tris/phosphate-buffered salt medium (75 mM mannitol, 25 mM sucrose, 100 mM KCl, 10 mM KH_2PO_4, 0.5 mM EDTA, 5 mM $MgCl_2$, 20 mM Tris, 1 mg/ml bovine serum albumin, pH 7.55). The measurement chamber was loaded with 1.5 ml of the respective buffer and heated to 37°C. Following equilibration, the reenergized samples were added and the chamber closed. At the end of each experiment, 100 ml of concentrated $N_2S_2O_4$ was added to remove oxygen. Calculations were performed with DatLab Analysis 2.1.

Analysis of oxidative stress

TRAP was measured as described (43). Briefly, cerebrum, cerebellum, liver and lung were removed and homogenized in 140 mM KCl/20 mM phosphate buffer pH 7.4 (KP buffer). The assay in a total volume of 3 ml phosphate-buffered saline pH 8.6 contained 20 mM 2,2′-azobis(2-methylpropionamidine) 2 HCl (ABAP) and 5 µM 3-aminophthalhydrazide (luminol) and was incubated at room temperature. The water-soluble vitamin E analog 6-hydroxy-2,5,7,8-tetramethylchroman-2-carboxylic acid (Trolox) was used as a standard.

TBARS were measured exactly as described (75) and reduced (GSH) and oxidized (GSSG) glutathione determined as in reference (76). MDA generated by iron/ascorbate-induced fatty acid oxidation was assayed as described (41) using homogenized tissue in a total volume of 100 µl KP buffer, 20 µM $FeCl_2$ and 250 µM ascorbate. The oxidation reaction was followed over 1 h at 37°C and stopped by the addition of 1 mM desferal and 200 µM butylated hydroxytoluene. TBARS were determined as described above.

For statistical evaluation, Student's *t*-test was applied. Experiments were repeated two to five times and results represented as means ± SD.

Supplementary Material

Refer to Web version on PubMed Central for supplementary material.

Acknowledgements

The authors are grateful to Dr Heimo Mairbaeurl for help with the Clark oxygen electrode, to Drs Antoine van Kampen and Emiel Ver Loren van Themaat (Amsterdam Medical Center) for evaluating the micro-array data and to Susanne Reusing for skillful technical assistance.

Funding

This work was supported by the FP6 European Union Project ‘Peroxisome’ (LSGH-CT-2004-512018).

References

1. Gorgas K, Teigler A, Komljenovic D, Just WW. The ether lipid-deficient mouse: tracking down plasmalogen functions. Biochim Biophys Acta. 2006; 1763:1511–1526. [PubMed: 17027098]
2. Thai TP, Rodemer C, Jauch A, Hunziker A, Moser A, Gorgas K, Just WW. Impaired membrane traffic in defective ether lipid biosynthesis. Hum Mol Genet. 2001; 10:127–136. [PubMed: 11152660]
3. Rodemer C, Thai TP, Brugger B, Gorgas K, Just W. Targeted disruption of ether lipid synthesis in mice. Adv Exp Med Biol. 2003; 544:355–368. [PubMed: 14713252]
4. Rodemer C, Thai TP, Brugger B, Kaercher T, Werner H, Nave KA, Wieland F, Gorgas K, Just WW. Inactivation of ether lipid biosynthesis causes male infertility, defects in eye development and optic nerve hypoplasia in mice. Hum Mol Genet. 2003; 12:1881–1895. [PubMed: 12874108]
5. Teigler A, Komljenovic D, Draguhn A, Gorgas K, Just WW. Defects in myelination, paranode organization and Purkinje cell innervation in the ether lipid-deficient mouse cerebellum. Hum Mol Genet. 2009; 18:1897–1908. [PubMed: 19270340]
6. Komljenovic D, Sandhoff R, Teigler A, Heid H, Just WW, Gorgas K. Disruption of blood-testis barrier dynamics in ether-lipid-deficient mice. Cell Tissue Res. 2009; 337:281–299. [PubMed: 19495798]
7. Moser HW. Molecular genetics of peroxisomal disorders. Front Biosci. 2000; 5:D298–D306. [PubMed: 10704429]
8. Wanders RJ, Waterham HR. Peroxisomal disorders I: biochemistry and genetics of peroxisome biogenesis disorders. Clin Genet. 2005; 67:107–133. [PubMed: 15679822]
9. Bams-Mengerink AM, Majoie CB, Duran M, Wanders RJ, Van Hove J, Scheurer CD, Barth PG, Poll-The BT. MRI of the brain and cervical spinal cord in rhizomelic chondrodysplasia punctata. Neurology. 2006; 66:798–803. [PubMed: 16567694]
10. Edwards RH. The neurotransmitter cycle and quantal size. Neuron. 2007; 55:835–858. [PubMed: 17880890]
11. Sudhof TC. The synaptic vesicle cycle. Annu Rev Neurosci. 2004; 27:509–547. [PubMed: 15217342]
12. Meinrenken CJ, Borst JG, Sakmann B. Local routes revisited: the space and time dependence of the Ca^{2+} signal for phasic transmitter release at the rat calyx of Held. J Physiol. 2003; 547:665–689. [PubMed: 12562955]
13. Geppert M, Goda Y, Hammer RE, Li C, Rosahl TW, Stevens CF, Sudhof TC. Synaptotagmin I: a major Ca^{2+} sensor for transmitter release at a central synapse. Cell. 1994; 79:717–727. [PubMed: 7954835]
14. Kummel D, Krishnakumar SS, Radoff DT, Li F, Giraudo CG, Pincet F, Rothman JE, Reinisch KM. Complexin cross-links prefusion SNAREs into a zigzag array. Nat Struct Mol Biol. 2011; 18:927–933. [PubMed: 21785414]
15. Sudhof TC, Rothman JE. Membrane fusion: grappling with SNARE and SM proteins. Science. 2009; 323:474–477. [PubMed: 19164740]

16. Jiang J, Amara SG. New views of glutamate transporter structure and function: advances and challenges. Neuropharmacology. 2011; 60:172–181. [PubMed: 20708631]
17. Ungewickell EJ, Hinrichsen L. Endocytosis: clathrin-mediated membrane budding. Curr Opin Cell Biol. 2007; 19:417–425. [PubMed: 17631994]
18. Zimmerberg J, Vogel SS, Chernomordik LV. Mechanisms of membrane fusion. Annu Rev Biophys Biomol Struct. 1993; 22:433–466. [PubMed: 8347997]
19. Chernomordik LV, Zimmerberg J. Bending membranes to the task: structural intermediates in bilayer fusion. Curr Opin Struct Biol. 1995; 5:541–547. [PubMed: 8528771]
20. Glaser PE, Gross RW. Plasmenylethanolamine facilitates rapid membrane fusion: a stopped-flow kinetic investigation correlating the propensity of a major plasma membrane constituent to adopt an HII phase with its ability to promote membrane fusion. Biochemistry. 1994; 33:5805–5812. [PubMed: 8180209]
21. Israelachvili JN, Mitchell DJ, Ninham BW. Theory of self-assembly of lipid bilayers and vesicles. Biochim Biophys Acta. 1977; 470:185–201. [PubMed: 911827]
22. Siegel DP. Energetics of intermediates in membrane fusion: comparison of stalk and inverted micellar intermediate mechanisms. Biophys J. 1993; 65:2124–2140. [PubMed: 8298039]
23. Inoue T, Wang Y, Jefferies K, Qi J, Hinton A, Forgac M. Structure and regulation of the V-ATPases. J Bioenerg Biomembr. 2005; 37:393–398. [PubMed: 16691471]
24. Bellocchio EE, Reimer RJ, Fremeau RT Jr, Edwards RH. Uptake of glutamate into synaptic vesicles by an inorganic phosphate transporter. Science. 2000; 289:957–960. [PubMed: 10938000]
25. Diagne A, Fauvel J, Record M, Chap H, Douste-Blazy L. Studies on ether phospholipids. II. Comparative composition of various tissues from human, rat and guinea pig. Biochim Biophys Acta. 1984; 793:221–231. [PubMed: 6712967]
26. Nagan N, Zoeller RA. Plasmalogens: biosynthesis and functions. Prog Lipid Res. 2001; 40:199–229. [PubMed: 11275267]
27. Fujita M, Kinoshita T. Structural remodeling of GPI anchors during biosynthesis and after attachment to proteins. FEBS Lett. 2010; 584:1670–1677. [PubMed: 19883648]
28. Honke K, Zhang Y, Cheng X, Kotani N, Taniguchi N. Biological roles of sulfoglycolipids and pathophysiology of their deficiency. Glycoconj J. 2004; 21:59–62. [PubMed: 15467400]
29. Ikezawa H. Glycosylphosphatidylinositol (GPI)-anchored proteins. Biol Pharm Bull. 2002; 25:409–417. [PubMed: 11995915]
30. Shimizu T. Lipid mediators in health and disease: enzymes and receptors as therapeutic targets for the regulation of immunity and inflammation. Annu Rev Pharmacol Toxicol. 2009; 49:123–150. [PubMed: 18834304]
31. Fan J, Sammalkorpi M, Haataja M. Formation and regulation of lipid microdomains in cell membranes: theory, modeling, and speculation. FEBS Lett. 2010; 584:1678–1684. [PubMed: 19854186]
32. Eggeling C, Ringemann C, Medda R, Schwarzmann G, Sandhoff K, Polyakova S, Belov VN, Hein B, von Middendorff C, Schonle A, et al. Direct observation of the nanoscale dynamics of membrane lipids in a living cell. Nature. 2009; 457:1159–1162. [PubMed: 19098897]
33. Pike LJ, Han X, Chung KN, Gross RW. Lipid rafts are enriched in arachidonic acid and plasmenylethanolamine and their composition is independent of caveolin-1 expression: a quantitative electrospray ionization/mass spectrometric analysis. Biochemistry. 2002; 41:2075–2088. [PubMed: 11827555]
34. Chamberlain LH, Burgoyne RD, Gould GW. SNARE proteins are highly enriched in lipid rafts in PC12 cells: implications for the spatial control of exocytosis. Proc Natl Acad Sci USA. 2001; 98:5619–5624. [PubMed: 11331757]
35. Lang T, Bruns D, Wenzel D, Riedel D, Holroyd P, Thiele C, Jahn R. SNAREs are concentrated in cholesterol-dependent clusters that define docking and fusion sites for exocytosis. EMBO J. 2001; 20:2202–2213. [PubMed: 11331586]
36. Nicholls DG. Bioenergetics and transmitter release in the isolated nerve terminal. Neurochem Res. 2003; 28:1433–1441. [PubMed: 14570388]

37. McMahon HT, Nicholls DG. Transmitter glutamate release from isolated nerve terminals: evidence for biphasic release and triggering by localized Ca^{2+} . J Neurochem. 1991; 56:86–94. [PubMed: 1670958]
38. Israel M, Lesbats B. Chemiluminescent determination of acetylcholine, and continuous detection of its release from torpedo electric organ synapses and synaptosomes. Neurochem Int. 1981; 3:81–90. [PubMed: 20487811]
39. Sanchez-Prieto J, Sihra TS, Nicholls DG. Characterization of the exocytotic release of glutamate from guinea-pig cerebral cortical synaptosomes. J Neurochem. 1987; 49:58–64. [PubMed: 2884280]
40. Engelmann B. Plasmalogens: targets for oxidants and major lipophilic antioxidants. Biochem Soc Trans. 2004; 32:147–150. [PubMed: 14748736]
41. Sindelar PJ, Guan Z, Dallner G, Ernster L. The protective role of plasmalogens in iron-induced lipid peroxidation. Free Radic Biol Med. 1999; 26:318–324. [PubMed: 9895222]
42. Spiteller G. Peroxyl radicals: inductors of neurodegenerative and other inflammatory diseases. Their origin and how they transform cholesterol, phospholipids, plasmalogens, polyunsaturated fatty acids, sugars, and proteins into deleterious products. Free Radic Biol Med. 2006; 41:362–387. [PubMed: 16843819]
43. Lissi E, Salim-Hanna M, Pascual C, del Castillo MD. Evaluation of total antioxidant potential (TRAP) and total antioxidant reactivity from luminol-enhanced chemiluminescence measurements. Free Radic Biol Med. 1995; 18:153–158. [PubMed: 7744297]
44. Dringen R. Glutathione metabolism and oxidative stress in neurodegeneration. Eur J Biochem. 2000; 267:4903. [PubMed: 10931171]
45. Lykkesfeldt J. Malondialdehyde as biomarker of oxidative damage to lipids caused by smoking. Clin Chim Acta. 2007; 380:50–58. [PubMed: 17336279]
46. Apostolou A, Shen Y, Liang Y, Luo J, Fang S. Armet, a UPR-upregulated protein, inhibits cell proliferation and ER stress-induced cell death. Exp Cell Res. 2008; 314:2454–2467. [PubMed: 18561914]
47. Oh-hashi K, Koga H, Ikeda S, Shimada K, Hirata Y, Kiuchi K. CRELD2 is a novel endoplasmic reticulum stress-inducible gene. Biochem Biophys Res Commun. 2009; 387:504–510. [PubMed: 19615339]
48. Hetz C, Bernasconi P, Fisher J, Lee AH, Bassik MC, Antonsson B, Brandt GS, Iwakoshi NN, Schinzel A, Glimcher LH, et al. Proapoptotic BAX and BAK modulate the unfolded protein response by a direct interaction with IRE1alpha. Science. 2006; 312:572–576. [PubMed: 16645094]
49. Walter P, Ron D. The unfolded protein response: from stress pathway to homeostatic regulation. Science. 2011; 334:1081–1086. [PubMed: 22116877]
50. Kauppinen RA, McMahon HT, Nicholls DG. Ca^{2+}-dependent and Ca^{2+}-independent glutamate release, energy status and cytosolic free Ca^{2+} concentration in isolated nerve terminals following metabolic inhibition: possible relevance to hypoglycaemia and anoxia. Neuroscience. 1988; 27:175–182. [PubMed: 2904664]
51. Dunant Y, Israel M. Neurotransmitter release at rapid synapses. Biochimie. 2000; 82:289–302. [PubMed: 10865118]
52. Grewer C, Gameiro A, Zhang Z, Tao Z, Braams S, Rauen T. Glutamate forward and reverse transport: from molecular mechanism to transporter-mediated release after ischemia. IUBMB Life. 2008; 60:609–619. [PubMed: 18543277]
53. Kanner BI, Bendahan A. Binding order of substrates to the sodium and potassium ion coupled L-glutamic acid transporter from rat brain. Biochemistry. 1982; 21:6327–6330. [PubMed: 6129891]
54. Paradies G, Petrosillo G, Paradies V, Ruggiero FM. Mitochondrial dysfunction in brain aging: role of oxidative stress and cardiolipin. Neurochem Int. 2011; 58:447–457. [PubMed: 21215780]
55. Cantrel C, Zachowski A, Geny B. Over-expression of the anti-apoptotic protein Bcl-2 affects membrane lipid composition in HL-60 cells. Lipids. 2009; 44:499–509. [PubMed: 19280241]
56. Kiebish MA, Han X, Cheng H, Lunceford A, Clarke CF, Moon H, Chuang JH, Seyfried TN. Lipidomic analysis and electron transport chain activities in C57BL/6J mouse brain mitochondria. J Neurochem. 2008; 106:299–312. [PubMed: 18373617]

57. Brostrom MA, Brostrom CO. Calcium dynamics and endoplasmic reticular function in the regulation of protein synthesis: implications for cell growth and adaptability. Cell Calcium. 2003; 34:345–363. [PubMed: 12909081]
58. Karar J, Dolt KS, Qadar Pasha MA. Endoplasmic reticulum stress response in murine kidney exposed to acute hypobaric hypoxia. FEBS Lett. 2008; 582:2521–2526. [PubMed: 18572019]
59. Ron D, Walter P. Signal integration in the endoplasmic reticulum unfolded protein response. Nat Rev Mol Cell Biol. 2007; 8:519–529. [PubMed: 17565364]
60. Hale CC, Ebeling EG, Hsu FF, Ford DA. The selective activation of the cardiac sarcolemmal sodium-calcium exchanger by plasmalogenic phosphatidic acid produced by phospholipase D. FEBS Lett. 1998; 422:247–251. [PubMed: 9490017]
61. Zoeller RA, Morand OH, Raetz CR. A possible role for plasmalogens in protecting animal cells against photosensitized killing. J Biol Chem. 1988; 263:11590–11596. [PubMed: 3403547]
62. Khaselev N, Murphy RC. Peroxidation of arachidonate containing plasmenyl glycerophosphocholine: facile oxidation of esterified arachidonate at carbon-5. Free Radic Biol Med. 2000; 29:620–632. [PubMed: 11033414]
63. Stadelmann-Ingrand S, Favreliere S, Fauconneau B, Mauco G, Tallineau C. Plasmalogen degradation by oxidative stress: production and disappearance of specific fatty aldehydes and fatty alpha-hydroxyaldehydes. Free Radic Biol Med. 2001; 31:1263–1271. [PubMed: 11705705]
64. Dunkley PR, Jarvie PE, Heath JW, Kidd GJ, Rostas JA. A rapid method for isolation of synaptosomes on Percoll gradients. Brain Res. 1986; 372:115–129. [PubMed: 3011205]
65. Gil C, Soler-Jover A, Blasi J, Aguilera J. Synaptic proteins and SNARE complexes are localized in lipid rafts from rat brain synaptosomes. Biochem Biophys Res Commun. 2005; 329:117–124. [PubMed: 15721282]
66. Krautkramer E, Giese SI, Gasteier JE, Muranyi W, Fackler OT. Human immunodeficiency virus type 1 Nef activates p21-activated kinase via recruitment into lipid rafts. J Virol. 2004; 78:4085–4097. [PubMed: 15047825]
67. Kauppinen RA, Nicholls DG. Synaptosomal bioenergetics. The role of glycolysis, pyruvate oxidation and responses to hypoglycaemia. Eur J Biochem. 1986; 158:159–165. [PubMed: 2874024]
68. Cousin MA, Robinson PJ. Two mechanisms of synaptic vesicle recycling in rat brain nerve terminals. J. Neurochem. 2000; 75:1645–1653. [PubMed: 10987846]
69. Ternaux JP, Chamoin MC. Enhanced chemiluminescent assays for acetylcholine. J Biolumin Chemilumin. 1994; 9:65–72. [PubMed: 8023705]
70. Hartree EF. Determination of protein: a modification of the Lowry method that gives a linear photometric response. Anal Biochem. 1972; 48:422–427. [PubMed: 4115981]
71. Bligh EG, Dyer WJ. A rapid method of total lipid extraction and purification. Can J Biochem Physiol. 1959; 37:911–917. [PubMed: 13671378]
72. Brugger B, Erben G, Sandhoff R, Wieland FT, Lehmann WD. Quantitative analysis of biological membrane lipids at the low picomole level by nano-electrospray ionization tandem mass spectrometry. Proc Natl Acad Sci USA. 1997; 94:2339–2344. [PubMed: 9122196]
73. Brugger B, Graham C, Leibrecht I, Mombelli E, Jen A, Wieland F, Morris R. The membrane domains occupied by glycosylphosphatidylinositol-anchored prion protein and Thy-1 differ in lipid composition. J Biol Chem. 2004; 279:7530–7536. [PubMed: 14660659]
74. Rouser G, Fkeischer S, Yamamoto A. Two dimensional then layer chromatographic separation of polar lipids and determination of phospholipids by phosphorus analysis of spots. Lipids. 1970; 5:494–496. [PubMed: 5483450]
75. Lindsey JA, Zhang HF, Kaseki H, Morisaki N, Sato T, Cornwell DG. Fatty acid metabolism and cell proliferation. VII. Antioxidant effects of tocopherols and their quinones. Lipids. 1985; 20:151–157. [PubMed: 3921792]
76. Boyne AF, Ellman GL. A methodology for analysis of tissue sulfhydryl components. Anal Biochem. 1972; 46:639–653. [PubMed: 4623507]

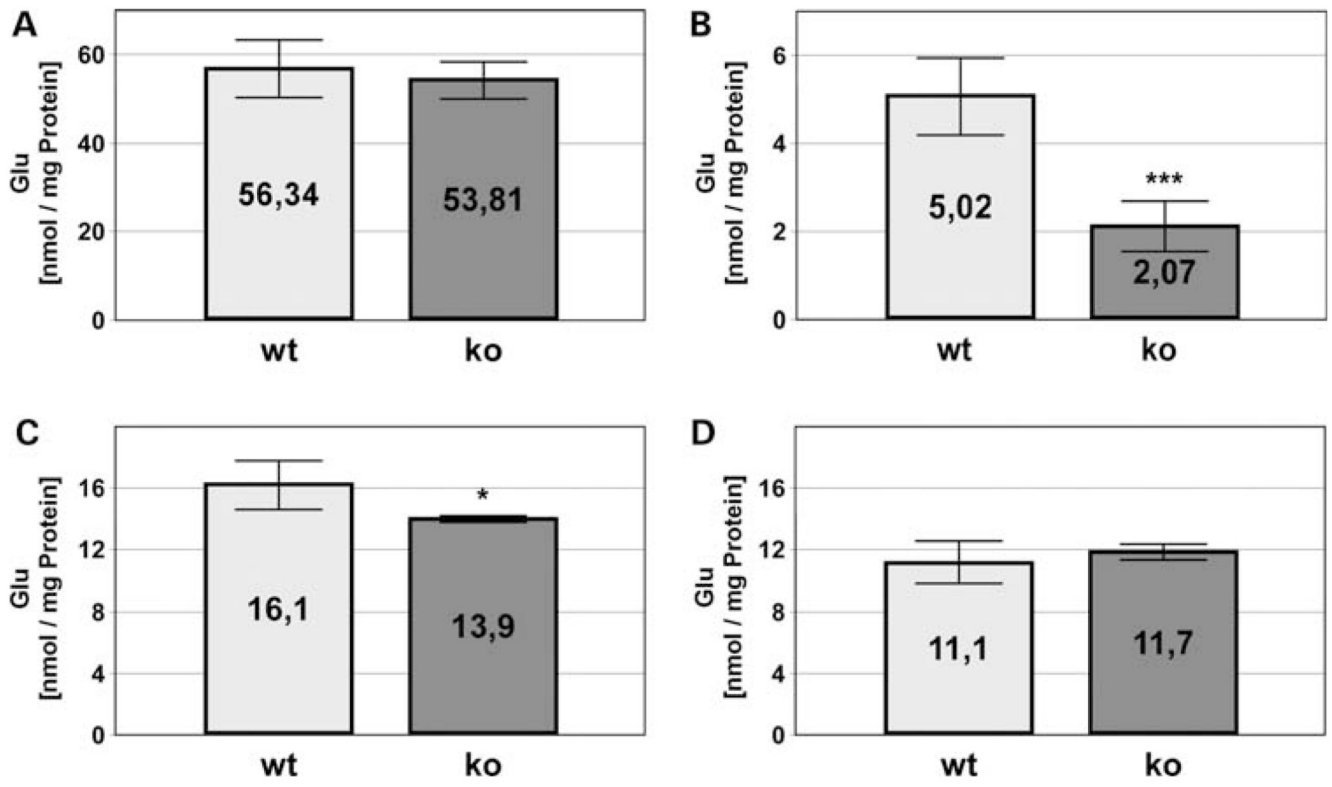

Figure 1.

Glu release from isolated cortical SYNs of wild-type (WT) and EL-deficient (KO) mouse brain. Total Glu content (0.5% Triton X-100) (**A**) and release in presence of 1.3 mM Ca^{2+} (**B** and **C**) and 1 mm ethylene glycol tetraacetic acid (EGTA) (**D**) from SYNs (400 μg) were determined. The Ca^{2+}-dependent release is shown in (B). Values represent means ± SD of three to five independent experiments. $*P \leq 0.05$, $***P \leq 0.001$.

Europe PMC Funders Author Manuscripts

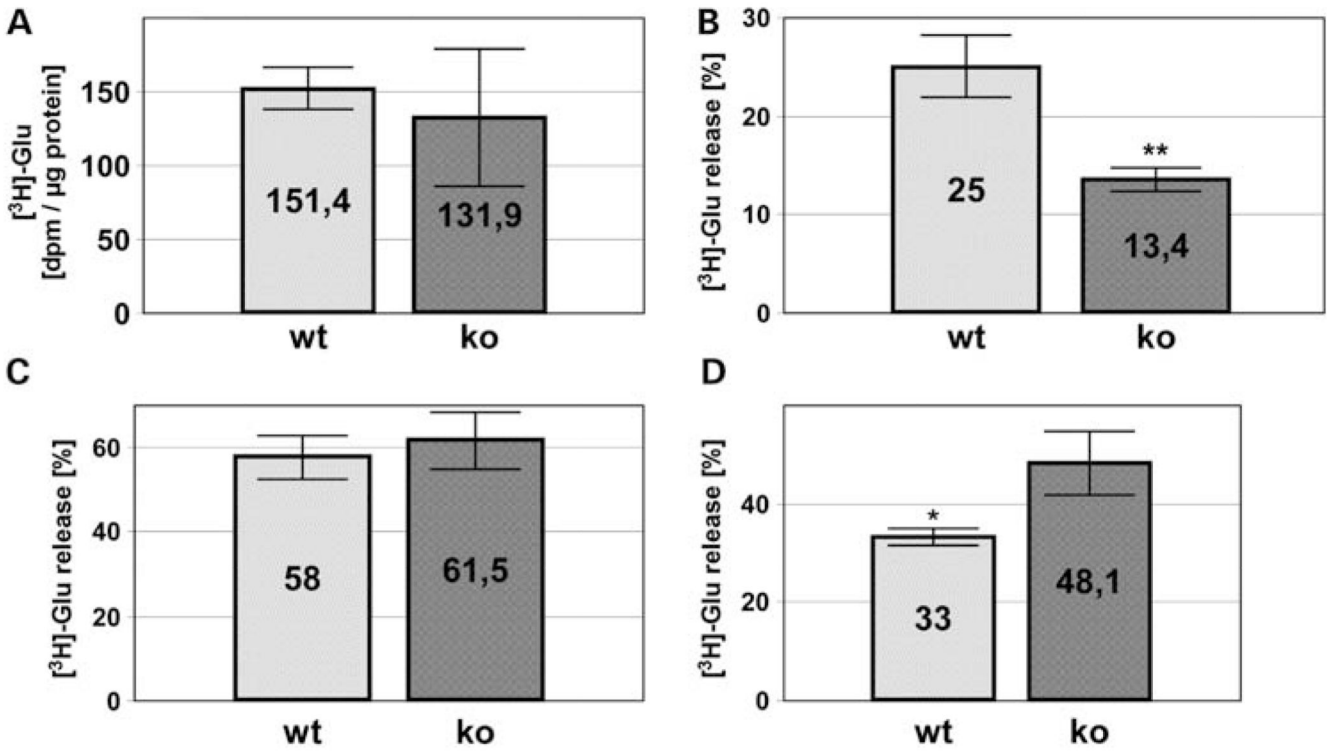

Figure 2.

[^{3}H]-Glutamate ([^{3}H]-Glu) uptake and release from isolated cortical SYNs of the wild-type (WT) and EL-deficient (KO) mouse brain. SYNs (300 µg) were incubated with 0.5 µCi [^{3}H]-Glu for 15 min prior to analyzing uptake (**A**) and release in the presence of 1.3 mM Ca^{2+} (**B** and **C**) and 1 mM EGTA (**D**). The Ca^{2+}-dependent release is shown in (B). Values represent means ± SD of three independent experiments. *$P \leq 0.05$, **$P \leq 0.01$.

Europe PMC Funders Author Manuscripts

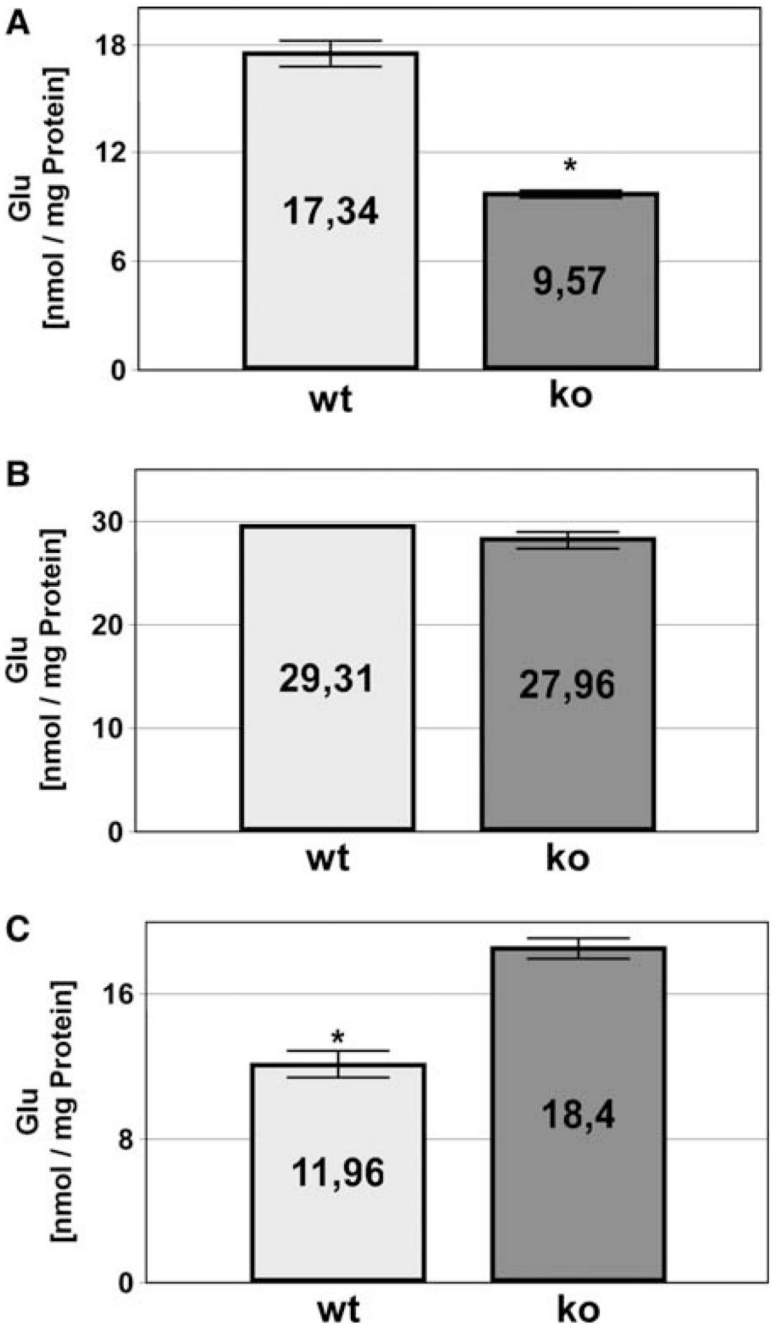

Figure 3.

Release of Glu from isolated cortical SYNs of wild-type (WT) and EL-deficient (KO) mouse brain in the presence of ionomycin. SYNs (400 μg) were incubated with 5 μM ionomycin prior to the addition of 1.3 mM Ca^{2+} (**B**) and 1 mM EGTA (**C**). The Ca^{2+}-dependent release obtained by the difference in release in the presence (B) and absence (C) of Ca^{2+} is shown in (**A**). Values represent means ± SD of three independent experiments. $^{*}P \leq 0.05$.

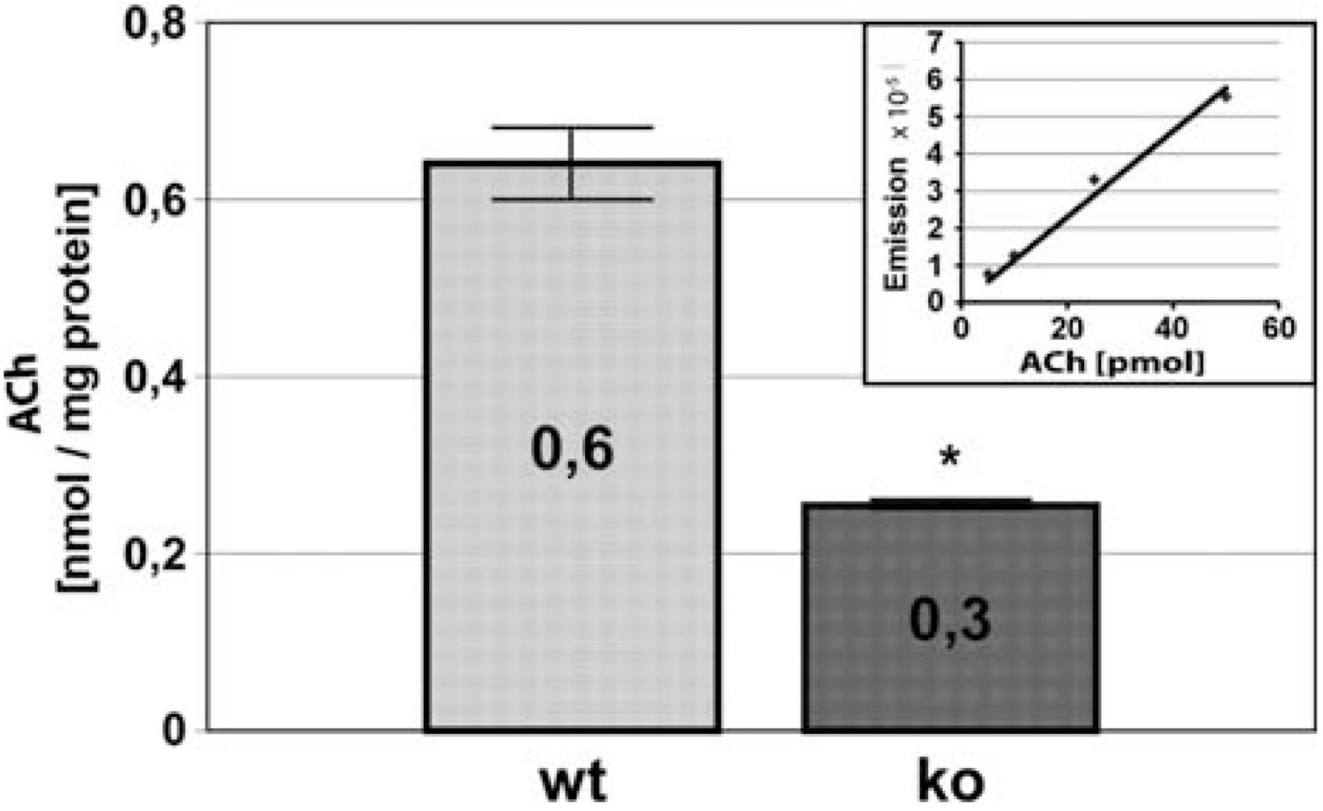

Figure 4.

ACh release from isolated cortical SYNs of wild-type (WT) and EL-deficient (KO) mouse brain. The Ca^{2+}-dependent release, i.e. the difference between the release from SYNs (400 μg) in the presence of 1.3 mM Ca^{2+} and 1 mM EGTA is shown. The inset demonstrates the linearity of the assay. Values represent means ± SD of three to five independent experiments. $^{**}P \leq 0.01$.

Europe PMC Funders Author Manuscripts

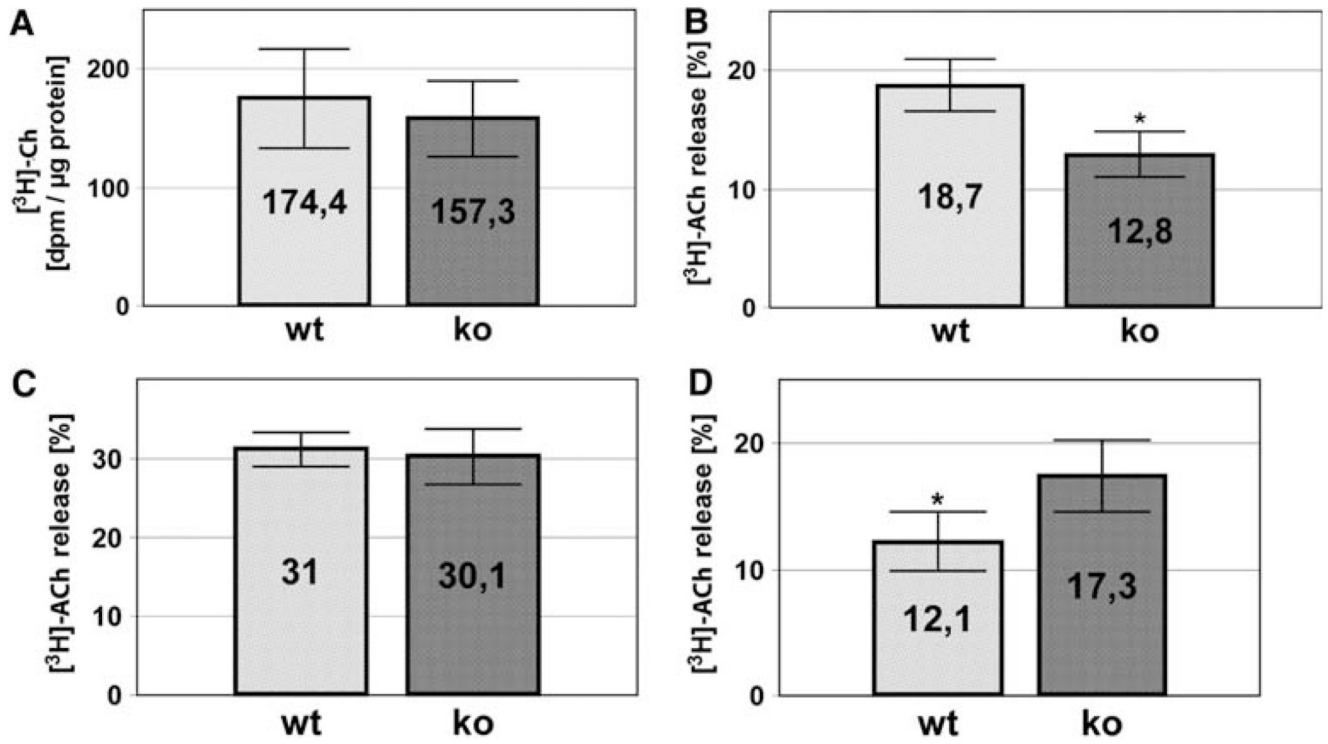

Figure 5.

[^{3}H]-Choline ([^{3}H]-Ch) uptake and [^{3}H]-acetylcholine ([^{3}H]-ACh) release from isolated cortical SYNs of wild-type (WT) and EL-deficient (KO) mouse brain. SYNs (300 µg) were incubated with 2 µCi of [^{3}H]-Ch for 30 min prior to analyzing uptake (**A**) and release in the presence of 1.3 mM Ca^{2+} (**B** and **C**) and 1 mM EGTA (**D**). The Ca^{2+}-dependent release is shown in (B). Values represent means ± SD of three independent experiments. *$P \leq 0.05$.

Europe PMC Funders Author Manuscripts

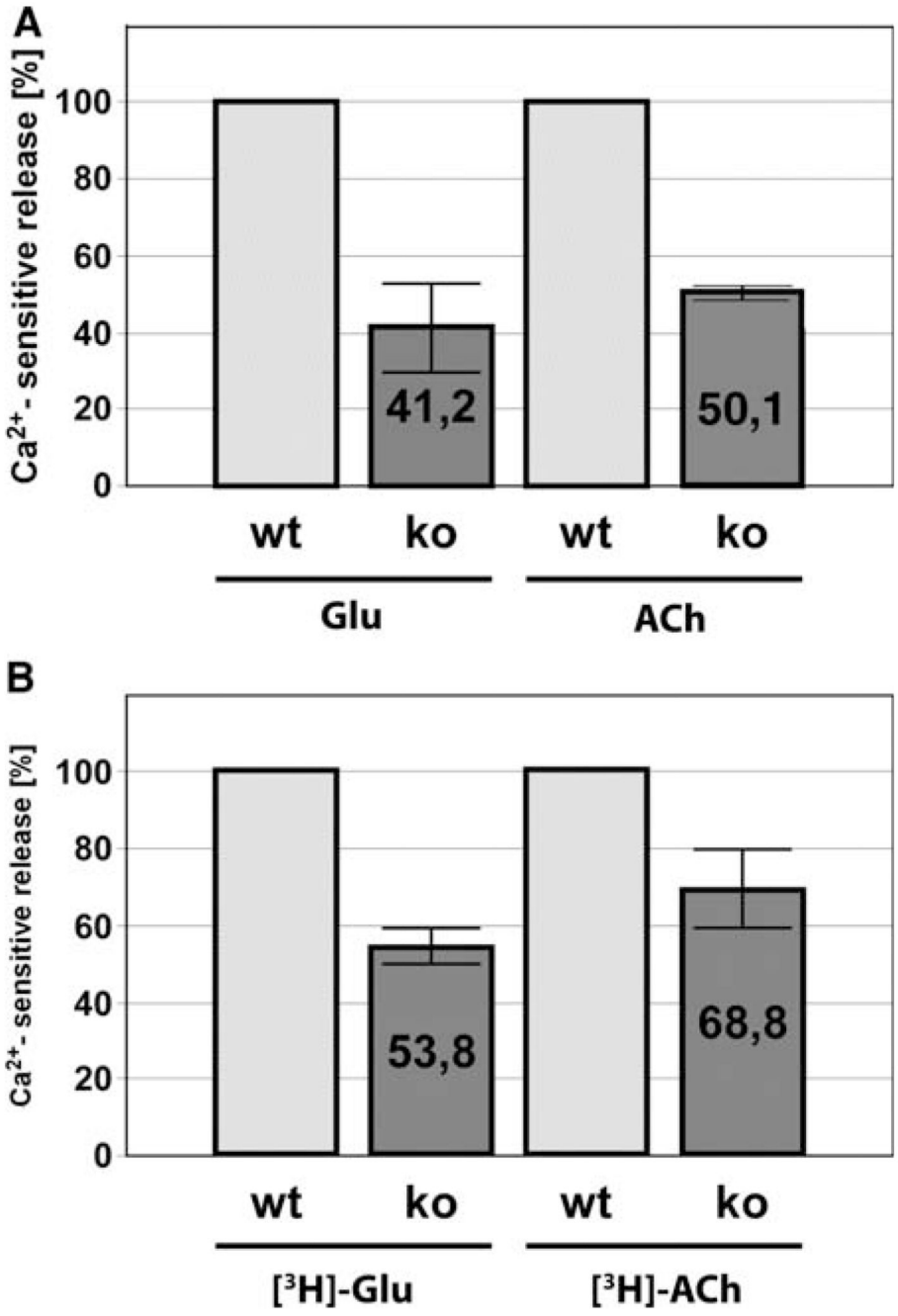

Figure 6.

Ca^{2+}-dependent release of endogenous Glu and ACh (**A**) as well as [^{3}H]-glutamate ([^{3}H]-Glu) and [^{3}H]-acetylcholine ([^{3}H]-ACh) (**B**) after [^{3} H]-GLU and [^{3}H]-choline ([^{3}H]-Ch) uptake into isolated cortical SYNs of wild-type (WT) and EL-deficient (KO) mouse brain. Values represent means ± SD of three to five independent experiments. $^{**}P \leq 0.01$.

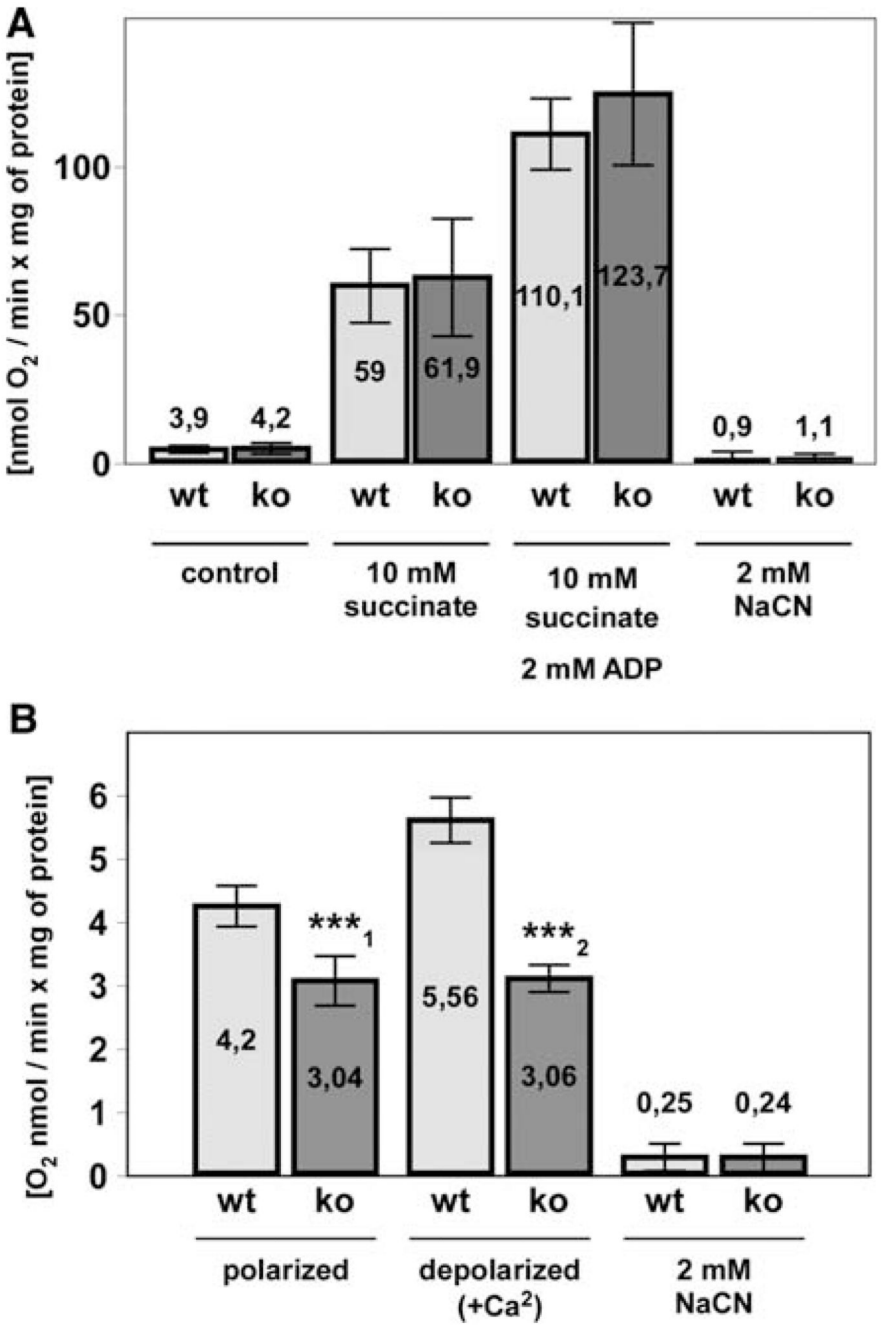

Figure 7.

Rate of respiration of free cortical mitochondria and SYNs of wildtype (WT) and EL-deficient (KO) mouse brain. Oxygen consumption of free mitochondria (125 μg) was determined in the presence of succinate, succinate plus adenosine diphosphate (ADP) and cyanide (**A**). Respiration of SYNs (750 μg) in the presence of 10 mM glucose and 1.3 mM Ca^{2+} (**B**). Note that under depolarizing conditions, WT SYNs increase respiratory rate by 25% compared with the polarized state, while KO SYNs are unable to do so. Values are means ± SD of three to five independent experiments. ***$P \leq 0.001$.

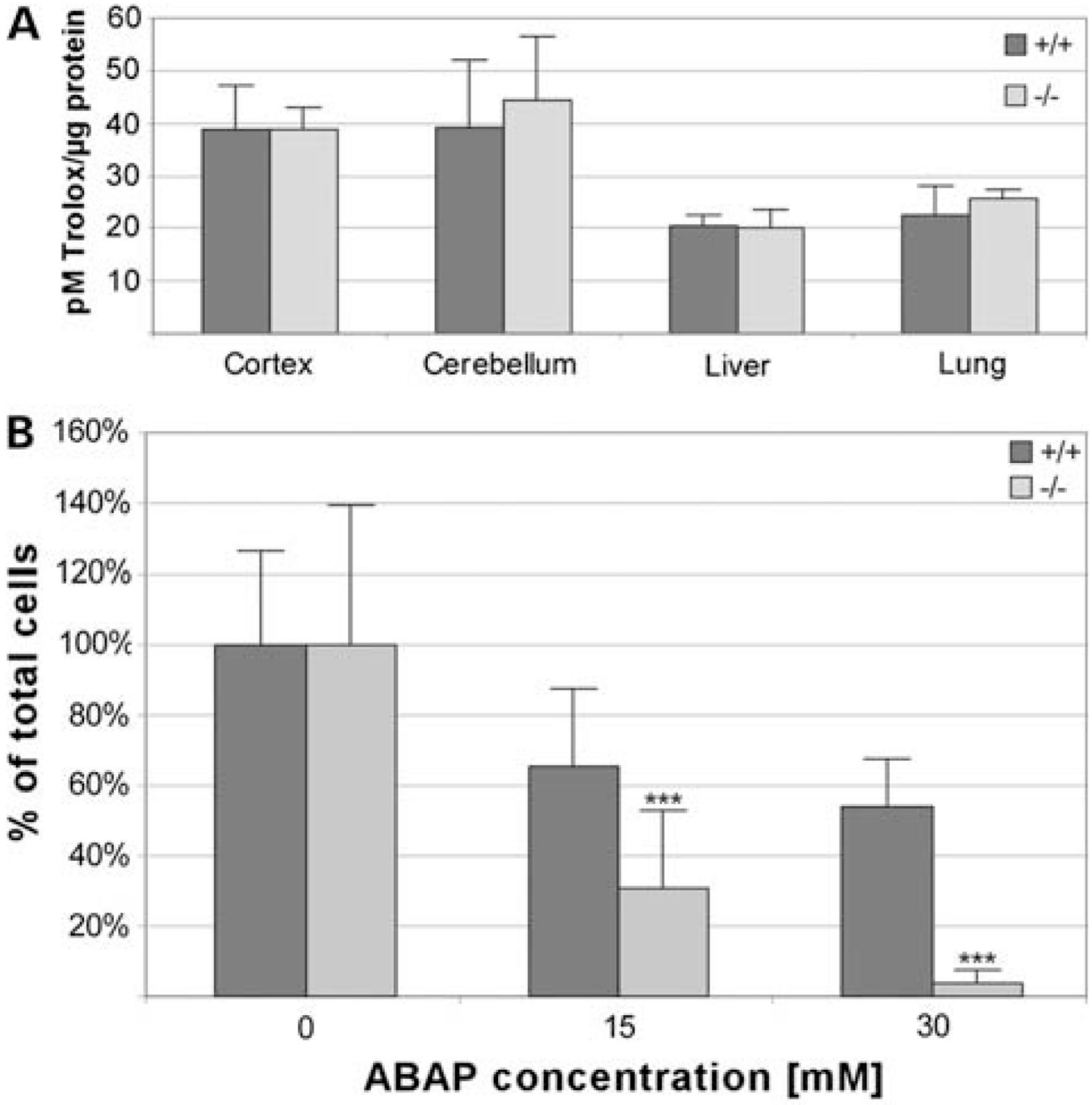

Figure 8.

TRAP of various tissues (**A**) of wild-type (WT) and EL-deficient (KO) mice and resistance of WT and KO mouse fibroblasts against 2,2′-azobis(2-methylpropionamidine) 2 HCl (ABAP)-induced oxidative stress (**B**). Values in (A) are means ± SD of three independent experiments. ***$P \leq 0.001$.

Europe PMC Funders Author Manuscripts

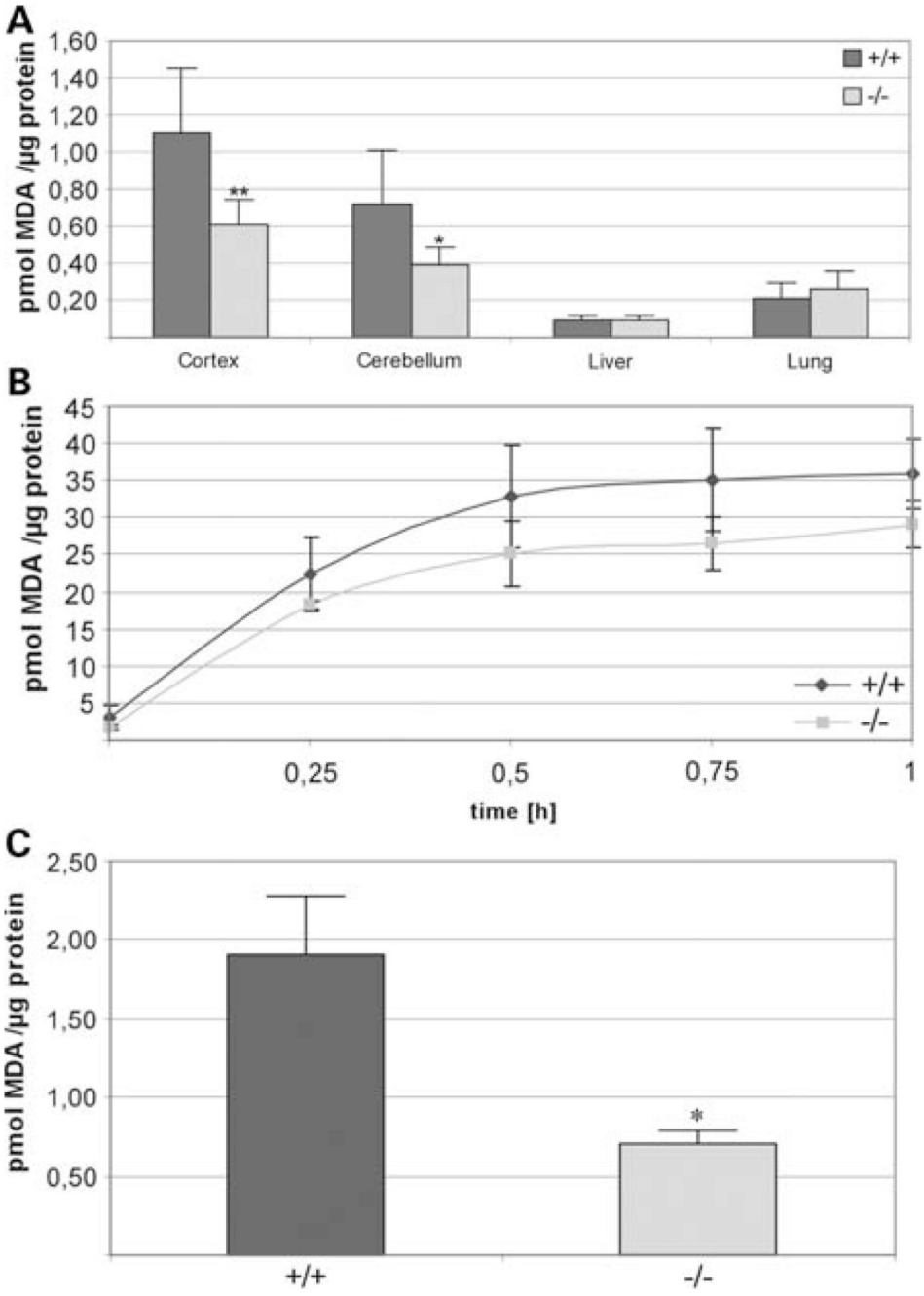

Figure 9.

TBARS of wild-type (+/+) and EL-deficient (−/−) tissues (**A**) as well as Fe^{2+}/ascorbate-induced TBARS in +/+ and −/− mouse brain cortical homogenate (**B**) and lipid extracts (**C**). The assay predominantly measures the concentration of MDA. Values represent means ± SD of three independent experiments. $*P \leq 0.05$, $**P \leq 0.025$.

Europe PMC Funders Author Manuscripts

Table 1

ATP and ADP content of re-energized cortical SYNs of wild-type (WT) and EL-deficient (KO) mouse brain

Condition	Tissue	ATP (nmol/mg of protein)	ADP (nmol/mg of protein)	ATP/ADP ratio
Re-energized	WT	3.11 ± 0.41	1.34 ± 0.3	2.37 ± 0.24
	KO	2.26 ± 0.35	1.24 ± 0.21	1.82 ± 0.12
% Change		−27*	−7	−23*

Values represent means ± SD of three independent experiments.

* $P \leq 0.05$.

Table 2

PE, plasmenylethanolamine (PL-PE) and cholesterol content of SYNs and synaptosomal LRMs of WT and EL-deficient (KO) mouse brain

m/z	Species	Synaptosomes (nmol/mg of protein)		LRMs (nmol/mg of protein)	
		WT	KO	WT	KO
PE					
718	34:1	2.33 ± 0.33	4.29 ± 0.33	5.66 ± 0.92	14.19 ± 1.35
740	36:4	3.44 ± 0.19	7.33 ± 0.66	2.90 ± 0.04	10.46 ± 1.63
744	36:2	3.00 ± 0.25	7.80 ± 0.71	5.54 ± 0.15	22.78 ± 3.51
746	36:1	3.91 ± 0.16	7.65. ± 0.34	17.21 ± 1.90	33.01 ± 5.58
764	38:6	10.74 ± 0.81	14.11 ± 1.92	7.68 ± 0.01	12.41 ± 2.18
768	38:4	34.56 ± 0.98	79.11 ± 6.42	26.35 ± 0.68	94.53 ± 14.6
792	40:6	55.09 ± 4.44	46.50 ± 5.32	35.91 ± 4.55	34.95 ± 6.77
796	40:4	5.41 ± 0.22	10.12 ± 1.27	7.99 ± 0.70	22.09 ± 3.20
Total		118.48	176.91	109.24	244.42
PL-PE					
702	16:1–18:1	6.29 ± 0.25	n.d.	31.51 ± 4.43	n.d.
	18:2–16:0				
724	16:1–20:4	3.48 ± 0.35	n.d.	3.06 ± 0.24	n.d.
728	18:2–18:1	7.31 ± 0.33	n.d.	47.64 ± 8.27	n.d.
	16:1–20:2				
730	18:1–18:1	7.19 ± 0.10	n.d.	66.84 ± 9.04	n.d.
	16:1–20:1				
748	16:1–22:6	9.96 ± 0.60	n.d.	6.64 ± 0.25	n.d.
750	18:2–20:4	6.30 ± 0.80	n.d.	11.19 ± 1.52	n.d.
	16:1–22:5				
752	16:1–22:4	13.08 ± 0.43	n.d.	29.43 ± 3.87	n.d.
	18:1–20:4				
756	18:2–20:1	2.55 ± 0.21	n.d.	26.18 ± 3.60	n.d.
	18:1–20:2				
758	18:1–20:1	1.78 ± 0.02	n.d.	26.09 ± 2.31	n.d.
	18:2–20:0				
774	18:2–22:6	4.51 ± 0.11	n.d.	2.82 ± 0.62	n.d.
776	18:1–22:6	21.07 ± 0.14	n.d.	23.69 ± 2.50	n.d.
778	18:2–22:4	5.52 ± 0.46	n.d.	11.29 ± 2.03	n.d.
	18:1–22:5				
780	18:1–22:4	5.95 ± 0.14	n.d.	20.93 ± 4.72	n.d.
Total		94.99		307.31	
Cholesterol		192.6 ± 28.7	160.0 ± 10.2	366.7 ± 35.1	353.3 ± 41.6

Values represent means ± SD of two to five independent experiments; n.d., not detected.